

Radiative decay of the $\Lambda^*(1520)$

M. Döring,^{1,†} E. Oset,^{1,‡} and Sourav Sarkar^{1,2,§}¹*Departamento de Física Teórica and IFIC, Centro Mixto Universidad de Valencia-CSIC, Institutos de Investigación de Paterna, Aptd. 22085, E-46071 Valencia, Spain*²*Variable Energy Cyclotron Centre, IIAF Bidhannagar, Kolkata 700064, India*

(Received 7 February 2006; revised manuscript received 27 September 2006; published 21 December 2006)

A recently developed nonperturbative chiral approach to dynamically generate the $3/2^-$ baryon resonances has been extended to investigate the radiative decays $\Lambda^*(1520) \rightarrow \gamma \Lambda(1116)$ and $\Lambda^*(1520) \rightarrow \gamma \Sigma^0(1193)$. We show that the $\Lambda^*(1520)$ decay into $\gamma \Lambda$ is an ideal test for the need of extra components of the resonance beyond those provided by the chiral approach since the largest meson-baryon components give no contribution to this decay. The case is different for $\gamma \Sigma$ decay, where the theory agrees with experiment, though the large uncertainties of these data call for more precise measurements. Some estimates of the weight of the needed genuine resonance component are made.

DOI: [10.1103/PhysRevC.74.065204](https://doi.org/10.1103/PhysRevC.74.065204)

PACS number(s): 25.20.Lj, 14.20.Gk, 24.10.Eq, 11.30.Rd

I. INTRODUCTION

New light has been brought into the study of the meson-baryon interaction by the unitary extensions of chiral perturbation theory ($U\chi PT$), showing that some well-known resonances qualify as being dynamically generated. In this picture the Bethe-Salpeter resummation of elementary interactions derived from chiral Lagrangians guarantees unitarity and leads at the same time to genuine nonperturbative phenomena such as poles of the scattering amplitude in the complex plane, which can be identified with resonances. Coupled channels play an essential role in this scheme, as the chiral Lagrangians provide the corresponding transitions within the multiplets, and even physically closed channels can contribute effectively. It is interesting to note that, even without chiral Lagrangians, the use of basic interactions for the coupled channels calls for an interpretation of some resonances such as the $\Lambda(1405)$ as quasibound states of the scattering problem [1,2].

After earlier studies in this direction explaining the $\Lambda(1405)$ and the $N^*(1535)$ as meson-baryon (MB) quasibound states [3–7] from the interaction of the meson octet of the π with the baryon octet of the N , new efforts have been undertaken [8,9] to investigate the low-lying $3/2^-$ baryonic resonances that decay in s wave into 0^- mesons (M) and $3/2^+$ baryons (B^*) of the decuplet. The latter particles, the 0^- mesons and $3/2^+$ baryons, provide the building blocks of the coupled channels needed in the study of the meson-baryon s -wave interaction in the $3/2^-$ channel. A parameter-free Lagrangian accounts for this interaction at lowest order and the model exhibits poles in the different isospin and strangeness channels in the complex \sqrt{s} plane, which have been identified with resonances such as $\Lambda^*(1520)$, $\Sigma^*(1670)$, and $\Delta^*(1700)$.

However, the $3/2^-$ resonances also have large branching ratios for ($0^-, 1/2^+$) MB decays in the d wave, in many cases being even larger than the s -wave branching ratio because of

the larger available phase space. For a realistic model that can serve to make reliable predictions in hadronic calculations, the d -wave channels corresponding to these decays should be included, as has been done recently in Ref. [10] for one of the $3/2^-$ resonances from Ref. [9], the $\Lambda^*(1520)$. For the $MB \rightarrow MB^*$ s -wave to d -wave and $MB \rightarrow MB$ d -wave to d -wave transitions, chiral symmetry does not fix the coupling strength and so free parameters necessarily enter the model. However, this freedom allows for a good reproduction of d -wave experimental data for $\bar{K}N \rightarrow \bar{K}N$ and $\bar{K}N \rightarrow \pi\Sigma$ via the $\Lambda^*(1520)$ (see Refs. [10,11]). Once the free parameters are determined by fitting to the experimental data of these reactions, the predictivity of the model can be tested for different data sets, as has been done in Ref. [11] for the reactions $K^-p \rightarrow \pi^0\pi^0\Lambda$, $K^-p \rightarrow \pi^+\pi^-\Lambda$, $\gamma p \rightarrow K^+K^-p$, and $\pi^-p \rightarrow K^0K^-p$, where good agreement with data has been found in all cases.

In the present study we extend the chiral coupled-channel approach—without introducing new parameters—to investigate the radiative decays $\Lambda^*(1520) \rightarrow \gamma \Lambda(1116)$ and $\Lambda^*(1520) \rightarrow \gamma \Sigma^0(1193)$ for which new experimental results exist [12]. These reactions are of particular interest because they provide further insight into the nature of the $\Lambda^*(1520)$: A pure dynamically generated resonance would be made out of meson-baryon components, a genuine resonance would be made of three constituent quarks, but an admixture of the two types is possible and in the real world nonexotic resonances have both components, although, by definition, the meson-baryon components would largely dominate in what we call dynamically generated resonances. Yet, even in this case it is interesting to see whether some experiments show that extra components beyond the meson-baryon ones are called for.

The radiative decay of the $\Lambda^*(1520)$ provides a clear example of this: In one of the decays, $\Lambda^*(1520) \rightarrow \gamma \Lambda(1116)$, isospin symmetry filters out the dominant channels $\pi\Sigma^*$ and $\pi\Sigma$ of the present approach so that a sizable fraction of the partial decay width could come from a genuine three-quark admixture. In contrast, these dominant channels add up in the isospin combination for the $\Lambda^*(1520) \rightarrow \gamma \Sigma^0(1193)$ reaction, and a match to the experimental data would point out the

[†]Electronic address: doering@ific.uv.es[‡]Electronic address: oset@ific.uv.es[§]Electronic address: sourav@veccal.ernet.in

dominant component for this channel being the quasibound meson-baryon system in coupled channels.

This situation is opposite to that of the quark model picture of Ref. [13], where the decay into $\gamma \Sigma^0(1193)$ is suppressed. This appears as a consequence of selection rules occurring in the limit in which only strange quarks are excited to p -wave bag orbits. Indeed, the photon de-excitation of the strange quark with a one-body operator does not affect the isospin of the u and d quarks and hence $I = 1$ baryons in the final state are forbidden in this limit [13]. However, as already stated, it is precisely the $\gamma \Sigma^0(1193)$ final state that appears enhanced in our hadronic interaction picture. We should also mention other quark models [14–19] that enlarge and complement Ref. [13], as well as algebraic models [20] where the $\Lambda(1520)$ radiative decay has been evaluated.

In the quark model of Ref. [13] it is shown that the partial decay widths of the Λ^* depend sensitively on the $q^4 \bar{q}$ admixture, which would correspond to meson-baryon components and, thus, could be related to the dynamically generated Λ^* .

The paper proceeds as follows. In Sec. II we give a short review of the underlying unitary chiral approach followed. In Sec. III the formalism for radiation decay is developed. Section IV shows the results and Sec. V presents a discussion of how to find the strength of the genuine resonance component. We conclude in Sec. VI with a summary of the relevant results found in the work.

II. FORMULATION

Before we proceed further, and to justify the procedure we follow, we present a general perspective of the ideas and techniques employed in the approach.

We begin by emphasizing that the method of dynamically generating resonances is not a tool to describe all resonances of the particle data group (PDG) [21]. Restricting ourselves to the baryonic resonances, thus far, only the low-lying $1/2^-$ and $3/2^-$ resonances qualify as such. The quantum numbers of these resonances are such that they can also be in principle interpreted as ordinary three-constituent-quark states with one quark in a p wave, which means that one should be ready to accept some three-constituent-quark components in the wave function. Conversely, the coupling of meson-baryon components to a seed of three constituent quarks is also unavoidable, as given for instance from the existence of meson-baryon decay channels. Nature will make this meson-baryon cloud more important in some cases than others, and those where the dress of the meson cloud overcomes the original three-constituent-quark seed are candidates to be well described in the chiral unitary approach and appear as what we call dynamically generated resonances in which the three-constituent-quark components are implicitly assumed to be negligible.

Then the following question arises: Which are the mesons and baryons that are used as building blocks in the chiral unitary approach and which can be dynamically generated? The answer to this is provided by exploiting the chiral theories in the large- N_c limit. The dynamically generated resonances appear as a solution of the Bethe-Salpeter equation and hence

it is the iteration of the kernel through loop diagrams that will lead to the appearance of these resonances. But these are subleading terms in the large- N_c counting that vanish in the limit of $N_c \rightarrow \infty$. Hence, the dynamically generated resonances disappear in a theoretical scheme when $N_c \rightarrow \infty$, and the resonances that remain are what we call genuine ones. In this sense, the $\Delta(1232)$ (and other baryons of the decuplet) is a genuine resonance that appears degenerate with the nucleon in the large- N_c limit [22]. This statement might seem to clash with a well-known historical fact, the dynamical generation of the $\Delta(1232)$ from the iteration of the crossed nucleon pole term in the Chew and Low theory [23]. However, attractive as the idea has always been, the input used in this approach, in particular the simplified πNN coupling, is at odds with present chiral Lagrangians and hence that old idea is no longer supported in present chiral approaches. A more modern and updated formulation of the problem, in accord with requirements of chiral dynamics, is given in Ref. [24]. There, the Δ , which qualifies as a genuine resonance, appears through a Castillejo-Dalitz-Dyson (CDD) pole [25] in the N/D formulation of Ref. [26].

The work of Ref. [27] corroborates this line of thought and traces back the “generation” of the Δ in the Chew-Low approach to the use of a unphysically large cutoff in Ref. [23] after proper kinematics is used.

There is much work related to the large- N_c limit of baryons [28–31]. A very important work on the meaning of the large- N_c limit and the classification of states into dynamically generated or genuine resonances is Ref. [32], where the author shows what large N_c means in practice, with some subtleties about the strict $N_c = \infty$. At the same time one shows that the ρ meson qualifies as a genuine resonance whereas the σ , $f_0(980)$, and $a_0(980)$ qualify as dynamically generated.

Next we discuss an issue of relevance: the relationship of the N/D method and the Bethe-Salpeter equation. This has been discussed in Refs. [26] and [7] but we summarize the problem here for the sake of clarity and completeness.

We start from the equation of unitarity in coupled channels and we shall work in the s wave for simplicity. (Generalization to other partial waves can be seen in Ref. [26].) Unitarity in coupled channels of meson-baryon is written as

$$\text{Im } T_{i,j} = T_{i,l} \sigma_l T_{l,j}^*, \quad (1)$$

where $\sigma_i \equiv 2M_l q_i / (8\pi \sqrt{s})$, with q_i the modulus of the c.m. three-momentum, and the subscripts i and j refer to the physical channels. This equation is most efficiently written in terms of the inverse amplitude as

$$\text{Im } T^{-1}(\sqrt{s})_{ij} = -\sigma(\sqrt{s})_i \delta_{ij}. \quad (2)$$

The unitarity relation in Eq. (2) gives rise to a cut in the T matrix of partial wave amplitudes, which is usually called the unitarity or right-hand cut. Hence, one can write a dispersion relation for $T^{-1}(\sqrt{s})$:

$$\begin{aligned} & T^{-1}(\sqrt{s})_{ij} \\ &= -\delta_{ij} \left\{ \tilde{a}_i(s_0) + \frac{s - s_0}{\pi} \int_{s_i}^{\infty} ds' \frac{\sigma(s')_i}{(s' - s - i\epsilon)(s' - s_0)} \right\} \\ & \quad + V^{-1}(\sqrt{s})_{ij}, \end{aligned} \quad (3)$$

where s_i is the value of the s variable at the threshold of channel i and $V^{-1}(\sqrt{s})_{ij}$ indicates other contributions coming from local and pole terms, as well as crossed-channel dynamics but *without* the right-hand cut. These extra terms can be taken directly from chiral perturbation theory (χPT) after requiring the *matching* of the general result to the χPT expressions if such a theory is available. Note also that

$$g(s)_i = \tilde{a}_i(s_0) + \frac{s - s_0}{\pi} \int_{s_i}^{\infty} ds' \frac{\sigma(s')_i}{(s' - s - i\epsilon)(s' - s_0)} \quad (4)$$

is the familiar scalar loop integral.

One can further simplify the notation by employing a matrix formalism. By introducing the matrices $g(s) = \text{diag}(g(s)_i)$, T , and V the latter defined in terms of the matrix elements T_{ij} and V_{ij} , the T matrix can be written as

$$T(\sqrt{s}) = [I - V(\sqrt{s}) \cdot g(s)]^{-1} \cdot V(\sqrt{s}), \quad (5)$$

which can be recast in a more familiar form as

$$T(\sqrt{s}) = V(\sqrt{s}) + V(\sqrt{s})g(s)T(\sqrt{s}). \quad (6)$$

This equation has the formal appearance of the Bethe-Salpeter equation (BSE). However, there is a peculiar feature worth noting: The term VgT of the equation is a product of functions $V(\sqrt{s})$, $g(s)$, and $T(\sqrt{s})$ whereas in the BSE using an ordinary \vec{r} -dependent potential, this term has an explicit d^4q integration involving V and T half off-shell. The appearance of V and T on-shell in Eq. (6) is a simple consequence of the dispersion relation of Eq. (3).

Note that $g(s)$ of Eq. (4) is nothing but the d^4q integral of a meson and baryon propagator (the check of the imaginary part is immediate). Hence, in simple words, we can say that the dispersion relation justifies a BSE in which the V and T are factorized on-shell outside the integral of the VgT term. Generalization of this technique to higher partial waves is done in Ref. [26]. In this case, there is a subtraction polynomial instead of the subtraction constant of Eq. (4), but in a narrow region around a resonance this can be taken as a constant.

There is a caveat in the argument given here: Equation (3) contains only the contribution of the imaginary part of the amplitude corresponding to the right-hand, physical cut. The unphysical, or left-hand, cut contribution is not taken into account. Therefore, there is an approximation involved. Yet, this is an approximation that is kept under control. In Ref. [26] a test was done of the contribution of the left-hand cut in meson-meson scattering with the conclusion that the contribution is small. More importantly, it is weakly energy dependent in the region of physical energies. This is the key to the success of the method explored here, since any constant contribution in a certain range of energies can be accommodated in terms of the subtraction constant that appears in the $g(s)$ function of Eq. (4) (see also a detailed discussion of the contribution of the left-hand cut in πN scattering in Ref. [24]). This finding is not unique to the former procedure since in some works [33,34] the crossed nucleon pole terms in πN scattering, which would lead to the left-hand cut contribution in the dispersion relation, are approximated by a local term.

The techniques discussed in this section have been applied successfully to the $\bar{K}N$ interaction in s waves [5] and p waves [35]. In this latter work, the kernel, V , has contact terms and

pole terms corresponding to the Λ , Σ , and $\Sigma^*(1385)$ particles. A similar procedure is done in Ref. [7] also for $\bar{K}N$ scattering and in Ref. [24] in the πN scattering case. The quality of the results and the sophistication of that latter model is equivalent to that of other successful relativistic approaches to πN such as those in Refs. [33,34], and fewer parameters are needed. In the case of the $\bar{K}N$ interaction of Refs. [5] and [35] a quite good description of the data was obtained with only one parameter.

To finalize this discussion we would like to clarify the differences between this version of the BSE based on the N/D method and dispersion relations from other versions of the BSE used in the literature. A discussion of different approaches to the BSE and its most often used three-dimensional reductions is presented in Ref. [36]. There is one main difference of the approach used here with respect to all others: In all of these other approaches the off-shell dependence of the potential plays a key role since it is responsible for the convergence of the integral involved in the VgT term of the BSE. In the present approach this is not needed since only the on-shell information of the potential enters the formalism. The aforementioned fourth-fold integral only involves the product of the meson and baryon propagators and is regularized with dimensional regularization, which is equivalent to using a dispersion relation with a subtraction. This procedure has a definite welcome feature since the results are invariant with respect to unitary transformations of the fields in the Lagrangian, and thus respect the equivalence theorem, something that does not occur in other variants of the BSE, as noted in Ref. [37]. The invariance of the results under these transformations is also satisfied by the K -matrix approach, which shares with our approach the use of the potential on-shell. The difference is that only the imaginary part of the integral of the two hadron propagators is kept in the K -matrix approach, whereas we also include the real part evaluated with dimensional regularization, or with a cutoff of natural size. This accounts for basic analytical properties of the scattering matrix, chiral logs, etc.

A. s -wave channels

Following Ref. [9], we briefly recall how the $\Lambda^*(1520)$ appears as a dynamically generated resonance in the s -wave interaction of the $3/2^+$ baryon decuplet with the 0^- meson octet. The lowest order term of the chiral Lagrangian relevant for the interaction is given by [22]

$$\mathcal{L} = -i\bar{T}^\mu \mathcal{D} T_\mu \quad (7)$$

[where we use the metric $g^{\mu\nu} = \text{diag}(1, -1, -1, -1)$], where T_{abc}^μ is the spin decuplet field and D^ν the covariant derivative given by

$$\mathcal{D}^\nu T_{abc}^\mu = \partial^\nu T_{abc}^\mu + (\Gamma^\nu)_a^d T_{dbc}^\mu + (\Gamma^\nu)_b^d T_{adc}^\mu + (\Gamma^\nu)_c^d T_{abd}^\mu, \quad (8)$$

where μ is the Lorentz index, a , b , and c are the SU(3) indices, and Γ^ν is the vector current. Let us recall the identification of the SU(3) components of T to the physical states [38,39]:

$$T^\mu = T_{ade} u^\mu, \quad \bar{T}_\mu = \bar{T}^{ade} \bar{u}_\mu, \quad T_{111} = \Delta^{++}, \\ T_{112} = \frac{\Delta^+}{\sqrt{3}}, \quad T_{122} = \frac{\Delta^0}{\sqrt{3}}, \quad T_{222} = \Delta^-, \quad T_{113} = \frac{\Sigma^{*+}}{\sqrt{3}},$$

$$T_{123} = \frac{\Sigma^{*0}}{\sqrt{6}}, T_{223} = \frac{\Sigma^{*-}}{\sqrt{3}}, T_{133} = \frac{\Xi^{*0}}{\sqrt{3}}, T_{233} = \frac{\Xi^{*-}}{\sqrt{3}},$$

$$T_{333} = \Omega^- . \quad (9)$$

The phase convention that we follow implies the phases for the isospin states, $|\pi^+\rangle = -|1, 1\rangle$, $|K^-\rangle = -|1/2, -1/2\rangle$, $|\Sigma^+\rangle = -|1, 1\rangle$.

In Ref. [9] the Lagrangian is expanded up to two mesons of incoming (outgoing) momentum $k(k')$, which leads to an interaction kernel of the form

$$V_{ij} = -\frac{1}{4f^2} C_{ij}(k^0 + k'^0) \quad (10)$$

for the s -wave transition amplitudes, as in Ref. [5]. For the quantum numbers strangeness $S = -1$ and isospin $I = 0$ the relevant channels are $\pi\Sigma^*$ and $K\Xi^*$ with the corresponding coefficients C_{ij} given in Sec. II B.

The matrix V is then used as the kernel of the BSE to obtain the unitary transition matrix [5]. This results in the matrix equation

$$T = (1 - VG)^{-1}V, \quad (11)$$

where G is a diagonal matrix representing the meson-baryon loop function given in Ref. [10]. The loop function contains an undetermined subtraction constant, which accounts for terms from higher order chiral Lagrangians that make it finite. In Ref. [10] the value of this constant has been fixed to $a_i = -2$ for a renormalization scale of $\mu = 700$ MeV. However, once the d -wave channels are introduced in the coupled-channel formalism, this constant will be allowed for fine-tuning within close limits.

B. Introduction of d -wave channels

As mentioned in Sec. I, a realistic coupled-channel model for the $\Lambda^*(1520)$ should also include meson-baryon channels of the octet of π with the octet of p because the branching ratios into $\bar{K}N$ and $\pi\Sigma$ are large. These latter states are then automatically in a d -wave state. For the present study we include the d -wave channels following Ref. [11]. In a previous work [10] the $\Lambda^*(1520)$ resonance was studied within a coupled-channel formalism by including the $\pi\Sigma^*$ and $K\Xi^*$ channels in s -wave and the $\bar{K}N$ and $\pi\Sigma$ channels in d -wave, leading to a good reproduction of the pole position of the $\Lambda^*(1520)$ of the scattering amplitudes. However, the use of the pole position to get the properties of the resonance is far from being accurate as soon as a threshold is opened close to the pole position on the real axis, which is the present case with the $\pi\Sigma^*$ channel.

Apart from that, in the approach of Ref. [10] some matrix elements in the kernel of the BSE were not considered. Therefore, a subsequent work [11] aimed at a more precise description of the physical processes involving the $\Lambda^*(1520)$ resonance. Hence, other possible tree-level transition potentials in the d wave are introduced here following Ref. [11]: $\bar{K}N \rightarrow \bar{K}N$, $\bar{K}N \rightarrow \pi\Sigma$, and $\pi\Sigma \rightarrow \pi\Sigma$. For these vertices, use is made of effective transition potentials that are proportional to the incoming and outgoing momentum squared

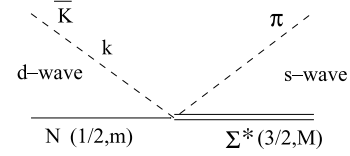


FIG. 1. The $\bar{K}N \rightarrow \pi\Sigma^*$ vertex.

to account for the d -wave character of the channels, which will be formalized in the following.

Consider the transition $\bar{K}N$ (d wave) to $\pi\Sigma^*$ (s wave) as shown in Fig. 1.

We start with an amplitude of the form

$$-it_{\bar{K}N \rightarrow \pi\Sigma^*} = -i\beta_{\bar{K}N} |\mathbf{k}|^2 [T^{(2)\dagger} \otimes Y_2(\hat{\mathbf{k}})]_{00}, \quad (12)$$

where $T^{(2)\dagger}$ is a (rank 2) spin transition operator defined by

$$\langle 3/2M | T_{\mu}^{(2)\dagger} | 1/2m \rangle = C(1/223/2; m\mu M) \langle 3/2 || T^{(2)\dagger} || 1/2 \rangle,$$

$Y_2(\hat{\mathbf{k}})$ is the spherical harmonic coupled to $T^{(2)\dagger}$ to produce a scalar, and \mathbf{k} is the momentum of the \bar{K} . The third component of spin of the initial nucleon and the final Σ^* are denoted by m and M , respectively, as indicated in the Clebsch-Gordan coefficients. The coupling strength β is not determined from theory and has to be fixed from experiment, as has been done in Ref. [11] with the results outlined in the following. Choosing appropriately the reduced matrix element we obtain

$$-it_{\bar{K}N \rightarrow \pi\Sigma^*} = -i\beta_{\bar{K}N} |\mathbf{k}|^2 C(1/223/2; m, M - m) \times Y_{2, m-M}(\hat{\mathbf{k}}) (-1)^{M-m} \sqrt{4\pi}. \quad (13)$$

In the same way the amplitude for the $\pi\Sigma$ (d -wave) to $\pi\Sigma^*$ (s -wave) transition is written as

$$-it_{\pi\Sigma \rightarrow \pi\Sigma^*} = -i\beta_{\pi\Sigma} |\mathbf{k}|^2 C(1/223/2; m, M - m) \times Y_{2, m-M}(\hat{\mathbf{k}}) (-1)^{M-m} \sqrt{4\pi} \quad (14)$$

and similarly for the rest of the other transitions mentioned. The angular dependence disappears in the loop integrations [10]. The loop function of the meson-baryon system in the d wave is strongly divergent, but an on-shell factorization can be achieved [10] by using arguments from the N/D method from Ref. [26] as explained in the previous section. The on-shell factorization ensures at the same time the unitarity of the amplitude after solving the BSE (11).

Denoting the $\pi\Sigma^*$, $K\Xi^*$, $\bar{K}N$, and $\pi\Sigma$ channels by 1, 2, 3, and 4, respectively, we write the kernel V of the BSE (11) as

$$V = \begin{pmatrix} C_{11}(k_1^0 + k_1^0) & C_{12}(k_1^0 + k_2^0) & \gamma_{13}q_3^2 & \gamma_{14}q_4^2 \\ C_{21}(k_2^0 + k_1^0) & C_{22}(k_2^0 + k_2^0) & 0 & 0 \\ \gamma_{13}q_3^2 & 0 & \gamma_{33}q_3^4 & \gamma_{34}q_3^2q_4^2 \\ \gamma_{14}q_4^2 & 0 & \gamma_{34}q_3^2q_4^2 & \gamma_{44}q_4^4 \end{pmatrix}, \quad (15)$$

with the on-shell c.m. momenta $q_i = \frac{1}{2\sqrt{s}} \sqrt{[s - (M_i + m_i)^2][s - (M_i - m_i)^2]}$, meson energy $k_i^0 = (s - M_i^2 + m_i^2)/2\sqrt{s}$, and baryon(meson) masses $M_i(m_i)$. The elements V_{11} , V_{12} , V_{21} , V_{22} come from the lowest order chiral Lagrangian involving the decuplet of baryons and the octet of pseudoscalar mesons, as discussed in Sec. II A; see also Ref. [9,40]. The coefficients C_{ij} obtained from

Eq. (7) are $C_{11} = \frac{-1}{f^2}$, $C_{21} = C_{12} = \frac{\sqrt{6}}{4f^2}$, and $C_{22} = \frac{-3}{4f^2}$, where f is $1.15f_\pi$, with f_π ($=93$ MeV) the pion decay constant, which is an average between f_π and f_K , as was used in Ref. [5] in the related problem of the dynamical generation of the $\Lambda(1405)$.

In the kernel V we neglect the elements V_{23} and V_{24} , which involve the tree-level interaction of the $K \Xi^*$ channel with the d -wave channels, because the $K \Xi^*$ threshold is far from the $\Lambda^*(1520)$ mass and its role in the resonance structure is far smaller than that of the $\pi \Sigma^*$. This is also the reason why the $K \Xi$ channel in the d wave is completely ignored.

In summary, the parameters of the model are five d -wave coupling strengths γ_{ij} . Additionally, the subtraction constants can be fine-tuned around their natural values of -2 and -8 for s -wave loops and d -wave loops, respectively. The fit to $\bar{K}N \rightarrow \bar{K}N$ and $\bar{K}N \rightarrow \pi \Sigma$ data has been performed in Ref. [11] and the results for the parameter values can be found there.

In the study of the radiative decay of the $\Lambda^*(1520)$ we will need only the coupling strengths of the resonance to its coupled channels at the resonance position [11]. The effective s -wave (d -wave) couplings $g_{\Lambda^*MB^*}(g_{\Lambda^*MB})$ are obtained by expanding the amplitude around the pole in a Laurent series. The residue is then identified with the coupling strength, as described in Sec. IV, and we display the result for the g s in the isospin $I = 0$ channel from Ref. [11] in Table I.

III. RADIATIVE DECAY

For the radiative decay of the $\Lambda^*(1520)$ we study the reactions shown in Fig. 2 corresponding to $\gamma Y \rightarrow \pi \Sigma^*$. We consider in the loops all the meson-baryon states of the coupled channels and couple the photon to the first loop as shown in Fig. 2. In the loop attached to the photon we can have either $\pi \Sigma^*$ or $K \Xi^*$, which couples to the $\Lambda^*(1520)$ in the s wave, or $\bar{K}N$, $\pi \Sigma$, which couple in the d wave. We show in the figure with the symbol T the diagrams that are accounted by the $T(i \rightarrow \pi \Sigma^*)$ amplitude with i any of the four channels $\pi \Sigma^*$, $K \Xi^*$, $\bar{K}N$, or $\pi \Sigma$. For the photon coupling we restrict ourselves to the Kroll-Ruderman (KR) and meson-pole (MP) coupling as shown in the figure. Formally, the photon should also be coupled to the meson and baryon components of the iteration of intermediate loops forming the $\Lambda^*(1520)$ but then the first loop vanishes for parity reasons (p wave and s or d wave in the first loop). For the same reason the coupling of the photon to the $\Lambda(\Sigma^0)$ initial baryon would vanish. The coupling of the γ to the baryon in the first loop vanishes in the heavy-baryon limit and is very small otherwise. A general discussion of issues of gauge invariance, chiral invariance, etc.,

TABLE I. Coupling strength of the dynamically generated $\Lambda^*(1520)$ to (MB^*) in the s wave and (MB) in the d wave [11].

$g_{\Lambda^*\pi\Sigma^*}$	$g_{\Lambda^*K\Xi^*}$	$g_{\Lambda^*\bar{K}N}$	$g_{\Lambda^*\pi\Sigma}$
0.91	-0.29	-0.54	-0.45

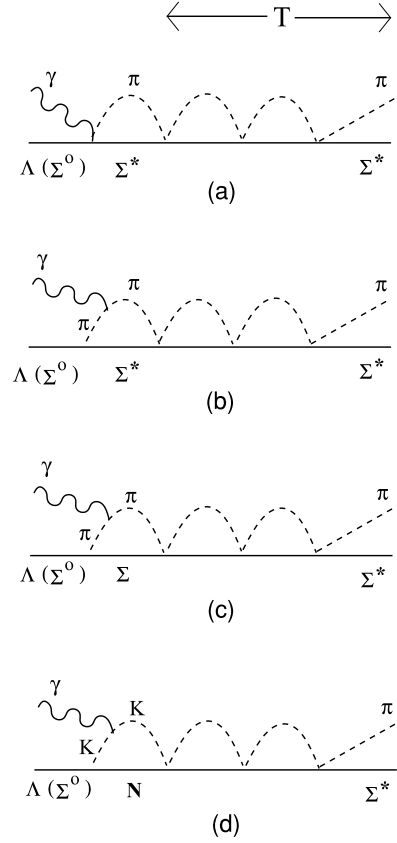


FIG. 2. Coupling of the photon to the $\Lambda^*(1520)$. Diagrams (a) and (b) show the coupling to a $\pi \Sigma^*$ loop, which enters together with the corresponding diagrams in the $K \Xi^*$ channel. The rescattering series that generates the pole of the $\Lambda^*(1520)$ in the complex scattering plane is symbolized by T . Diagrams (c) and (d) show the γ coupling to the d waves of the resonance.

within the context of unitarized chiral theories, can be found in Refs. [41,42]. In Ref. [41] the authors proved that gauge invariance is preserved when the photon is coupled to internal as well as external lines and vertices. An additional discussion on this issue is given in Ref. [42]. According to these findings our present approach fulfills gauge invariance with errors of the order of 2% from the approximations done.

For the diagrams from Fig. 2, the MBB^* vertices and the KR coupling γMBB^* are needed, for which we use the Lagrangian from Ref. [39], with the part relevant for the present reaction given by

$$\begin{aligned} \mathcal{L} &= \mathcal{C}(\bar{T}_\mu A^\mu B + \bar{B} A_\mu T^\mu) \\ &= \mathcal{C} \left(\sum_{a,b,c,d,e}^{1,\dots,3} \epsilon_{abc} \bar{T}^{ade} \bar{u}_\mu A_d^{b,\mu} B_e^c \right. \\ &\quad \left. + \sum_{a,b,c,d,e}^{1,\dots,3} \epsilon^{abc} \bar{B}_c^e A_{b,\mu}^d T_{ade} u^\mu \right), \end{aligned} \quad (16)$$

with the same phase conventions as in Eq. (7) and the spin and flavor structure as given in Ref. [9] and Eq. (9). In Eq. (16),

the axial current is expanded up to one meson field,

$$A^\mu = \frac{i}{2}(\xi \partial^\mu \xi^\dagger - \xi^\dagger \partial^\mu \xi) \xrightarrow{\text{one } \Phi} \frac{\partial^\mu \Phi}{\sqrt{2} f_\pi}, \quad (17)$$

$$\xi = \exp\left(\frac{i\Phi}{\sqrt{2} f_\pi}\right);$$

Φ , B , and \bar{B} are the standard meson and baryon SU(3) fields [43]; and $f_\pi = 93$ MeV. For the KR vertex $\gamma M B B^*$, we couple the photon by minimal substitution to Eq. (16). The coupling strength \mathcal{C} is determined from the $\Delta(1232)$ decay,

$$\frac{\mathcal{C}}{\sqrt{2} f_\pi} = \frac{f_{\Delta\pi N}^*}{m_\pi}, \quad (18)$$

with $f_{\Delta\pi N}^* = 2.13$. The SU(3) breaking in the decuplet beyond that from the different masses is of the order of 30%, as a fit of Eq. (16) to the partial decay widths of $\Delta(1232)$, Σ^* , and Ξ^* shows [39,44]. In the present study, we do not take this breaking into account to be consistent with the model for the dynamical generation of the $\Lambda^*(1520)$ where the SU(3) breaking from other sources than mass differences is also neglected.

From Eq. (16) and from the minimal coupling with the photon, Feynman rules for $(\Lambda, \Sigma^0) \rightarrow M B^*$, $\gamma(\Lambda, \Sigma^0) \rightarrow M B^*$, and the ordinary $\gamma M M$ vertices are obtained in which the meson momentum \mathbf{q} is defined as outgoing and the photon momentum \mathbf{k} as incoming:

$$(-it)_{B \rightarrow M(\mathbf{q})B^*} = \frac{d f_{\Delta\pi N}^*}{m_\pi} \mathbf{S}^\dagger \cdot \mathbf{q},$$

$$(-it \cdot \boldsymbol{\epsilon})_{KR} = -\frac{e c d f_{\Delta\pi N}^*}{m_\pi} \mathbf{S}^\dagger \cdot \boldsymbol{\epsilon}, \quad (19)$$

$$(-it \cdot \boldsymbol{\epsilon})_{\gamma(\mathbf{k})M(\mathbf{q}-\mathbf{k}) \rightarrow M(\mathbf{q})} = i e c (2\mathbf{q} - \mathbf{k}) \cdot \boldsymbol{\epsilon},$$

with the coefficients d given in Table II.

In Eqs. (19) $e > 0$ is the electron charge and $c = +1$ ($c = -1$) for π^+ , K^+ (π^- , K^-) and $c = 0$ for processes with neutral mesons. The photon with the polarization ϵ^μ is real and we use the Coulomb gauge $\epsilon^0 = 0$, $\boldsymbol{\epsilon} \cdot \mathbf{k} = 0$.

For the first diagram in Fig. 2 in which $\pi^- \Sigma^{*+}$, $\pi^+ \Sigma^{*-}$, and $K^+ \Xi^{*-}$ couple in the s wave to T , we construct the amplitude for the reactions $\gamma \Lambda \rightarrow \pi \Sigma^*$ and $\gamma \Sigma \rightarrow \pi \Sigma^*$ with isospin $I = 0$. For this purpose, an isospin combination for the first loop is constructed according to

$$|\pi \Sigma^*, I = 0\rangle = -\frac{1}{\sqrt{3}} |\pi^+ \Sigma^{*-}\rangle - \frac{1}{\sqrt{3}} |\pi^0 \Sigma^{*0}\rangle$$

$$+ \frac{1}{\sqrt{3}} |\pi^- \Sigma^{*+}\rangle,$$

$$|K \Xi^*, I = 0\rangle = \frac{1}{\sqrt{2}} |K^+ \Xi^{*-}\rangle - \frac{1}{\sqrt{2}} |K^0 \Xi^{*0}\rangle, \quad (20)$$

TABLE II. Coefficients d for the Feynman rule [Eq. (19)] with Λ or Σ^0 in the initial state.

	$\pi^- \Sigma^{*+}$	$\pi^+ \Sigma^{*-}$	$K^+ \Xi^{*-}$
$d, \Lambda \rightarrow M B^*$	$-\frac{1}{\sqrt{2}}$	$\frac{1}{\sqrt{2}}$	$\frac{1}{\sqrt{2}}$
$d, \Sigma^0 \rightarrow M B^*$	$-\frac{1}{\sqrt{6}}$	$-\frac{1}{\sqrt{6}}$	$-\frac{1}{\sqrt{6}}$

with the phase conventions as previously noted. Note that states with neutral mesons do not contribute to the loops. Using the Feynman rules from Eq. (19) gives the results [indicating, e.g., $\pi \Sigma^*$ in the first loop by $(\pi \Sigma^*)$]

$$(-it \cdot \boldsymbol{\epsilon})_{KR}^{(I=0)} [\gamma \Lambda \rightarrow (\pi \Sigma^*) \xrightarrow{\Lambda^*} \pi \Sigma^*] = 0,$$

$$(-it \cdot \boldsymbol{\epsilon})_{KR}^{(I=0)} [\gamma \Lambda \rightarrow (K \Xi^*) \xrightarrow{\Lambda^*} \pi \Sigma^*] = -\frac{e f_{\Delta\pi N}^*}{2 m_\pi} \times G_2 T^{(21)} \mathbf{S}^\dagger \cdot \boldsymbol{\epsilon},$$

$$(-it \cdot \boldsymbol{\epsilon})_{KR}^{(I=0)} [\gamma \Sigma^0 \rightarrow (\pi \Sigma^*) \xrightarrow{\Lambda^*} \pi \Sigma^*] = -\frac{\sqrt{2} e f_{\Delta\pi N}^*}{3 m_\pi} \times G_1 T^{(11)} \mathbf{S}^\dagger \cdot \boldsymbol{\epsilon},$$

$$(-it \cdot \boldsymbol{\epsilon})_{KR}^{(I=0)} [\gamma \Sigma^0 \rightarrow (K \Xi^*) \xrightarrow{\Lambda^*} \pi \Sigma^*] = \frac{e f_{\Delta\pi N}^*}{2\sqrt{3} m_\pi} \times G_2 T^{(21)} \mathbf{S}^\dagger \cdot \boldsymbol{\epsilon}, \quad (21)$$

with $T^{(ij)}$ being the matrix element obtained from the BSE (11) with the channel ordering (ij) as in Eq. (15). In Eqs. (21), G_1 and G_2 are the ordinary loop functions for $\pi \Sigma^*$ and $K \Xi^*$ given by

$$G_i = \int \frac{d^3 \mathbf{q}}{(2\pi)^3} \frac{1}{2\omega} \frac{1}{\sqrt{s} - \omega(\mathbf{q}) - E(\mathbf{q}) + i\epsilon} \quad (22)$$

with the invariant scattering energy \sqrt{s} and meson and baryon energy ω and E , respectively. For the regularization a cutoff Λ is used. This cutoff is determined such that the G_i functions of Eq. (22) have the same value as obtained in [11] using dimensional regularization. For this purpose we match the $M B^*$ loop function in both regularization schemes (dimensional and cutoff) at $s^{1/2} = 1520$ MeV, which results in $\Lambda_{\pi \Sigma^*} = 418$ MeV for the $\pi \Sigma^*$ channel. This value is then used as the cutoff for Eq. (22). For the $K \Xi^*$ channel such a matching is not possible at energies so far below the $K \Xi^*$ threshold, and we set $\Lambda_{K \Xi^*} = 500$ MeV. In any case, the final numbers are almost independent of the value of $\Lambda_{K \Xi^*}$, first, because the contribution is tiny and, second, because the cutoff dependence of the s -wave loops is moderate.

To evaluate the contribution of the meson-pole term in the second diagram of Fig. 2, we must project the operator $\boldsymbol{\epsilon} \cdot (2\mathbf{q} - \mathbf{k}) \mathbf{S}^\dagger \cdot (\mathbf{q} - \mathbf{k})$ onto the s wave; for this we neglect \mathbf{k} , which is relatively small in the radiative decay. (The numerical test keeping the \mathbf{k} terms proves this to be a very good approximation.) Then, we get as a projection $\mathbf{S}^\dagger \cdot \boldsymbol{\epsilon} \frac{2}{3} \mathbf{q}^2$ and we have a new loop function

$$\tilde{G}_i = i \int \frac{d^4 q}{(2\pi)^4} \frac{\mathbf{q}^2}{(q-k)^2 - m_i^2 + i\epsilon} \frac{1}{q^2 - m_i^2 + i\epsilon}$$

$$\times \frac{1}{P^0 - q^0 - E_i(\mathbf{q}) + i\epsilon}$$

$$= - \int \frac{d^3 \mathbf{q}}{(2\pi)^3} \frac{\mathbf{q}^2}{2\omega_i \omega'_i} \frac{1}{k + \omega_i + \omega'_i} \frac{1}{k - \omega_i - \omega'_i + i\epsilon}$$

$$\times \frac{1}{\sqrt{s} - \omega_i - E_i(\mathbf{q}) + i\epsilon} \frac{1}{\sqrt{s} - k - \omega'_i - E_i(\mathbf{q}) + i\epsilon}$$

$$\times [(\omega_i + \omega'_i)^2 + (\omega_i + \omega'_i)(E_i(\mathbf{q}) - \sqrt{s}) + k\omega'_i], \quad (23)$$

where ω_i and ω'_i are the energies of the mesons of mass m_i at momentum \mathbf{q} and $\mathbf{q} - \mathbf{k}$, respectively, k is the energy of the on-shell photon, and E_i is the energy of the decuplet baryon. For the regularization of the loop we use the same cutoffs as for Eq. (22). The diagrams with meson-pole terms can be easily incorporated by changing $G_i \rightarrow G_i + \frac{2}{3} \tilde{G}_i$ in Eq. (21), resulting in

$$\begin{aligned}
(-it \cdot \boldsymbol{\epsilon})_{\text{KR+MP}}^{(I=0)}[\gamma \Lambda \rightarrow (\pi \Sigma^*) \xrightarrow{\Lambda^*} \pi \Sigma^*] &= 0, \\
(-it \cdot \boldsymbol{\epsilon})_{\text{KR+MP}}^{I=0}[\gamma \Lambda \rightarrow (K \Xi^*) \xrightarrow{\Lambda^*} \pi \Sigma^*] \\
&= -\frac{e}{2} \frac{f_{\Delta\pi N}^*}{m_\pi} (G_2 + \frac{2}{3} \tilde{G}_2) T^{(21)} \mathbf{S}^\dagger \cdot \boldsymbol{\epsilon}, \\
(-it \cdot \boldsymbol{\epsilon})_{\text{KR+MP}}^{(I=0)}[\gamma \Sigma^0 \rightarrow (\pi \Sigma^*) \xrightarrow{\Lambda^*} \pi \Sigma^*] \\
&= -\frac{\sqrt{2}e}{3} \frac{f_{\Delta\pi N}^*}{m_\pi} (G_1 + \frac{2}{3} \tilde{G}_1) T^{(11)} \mathbf{S}^\dagger \cdot \boldsymbol{\epsilon}, \\
(-it \cdot \boldsymbol{\epsilon})_{\text{KR+MP}}^{(I=0)}[\gamma \Sigma^0 \rightarrow (K \Xi^*) \xrightarrow{\Lambda^*} \pi \Sigma^*] \\
&= \frac{e}{2\sqrt{3}} \frac{f_{\Delta\pi N}^*}{m_\pi} (G_2 + \frac{2}{3} \tilde{G}_2) T^{(21)} \mathbf{S}^\dagger \cdot \boldsymbol{\epsilon}. \quad (24)
\end{aligned}$$

A. Radiative decay from d -wave loops

The third and fourth diagram in Fig. 2 show the photon coupling to the d -wave components of the $\Lambda^*(1520)$. The first loop implies two p -wave and one d -wave couplings, which lead to a nontrivial angular momentum structure. Note that there is no coupling of the KR type because the combination of s - and d -wave couplings vanishes by parity in the loop integration.

The MBB p -wave coupling is obtained from the lowest order chiral meson-baryon Lagrangian [43], which leads to the Feynman rule (for meson momentum \mathbf{p} outgoing)

$$(-it) = i\mathcal{L} = -\frac{\sqrt{2}}{f_\pi} \boldsymbol{\sigma} \cdot \mathbf{p} \left(a \frac{D+F}{2} + b \frac{D-F}{2} \right), \quad (25)$$

with a and b given in Table III, where only the channels including charged mesons are denoted.

TABLE III. Coefficients a and b for the Feynman rule [Eq. (25)] outgoing meson momentum.

	$\pi^- \Sigma^+$	$\pi^+ \Sigma^-$	$K^- p$
$a, \Lambda \rightarrow MB$	$\frac{1}{\sqrt{6}}$	$\frac{1}{\sqrt{6}}$	$-\sqrt{\frac{2}{3}}$
$b, \Lambda \rightarrow MB$	$\frac{1}{\sqrt{6}}$	$\frac{1}{\sqrt{6}}$	$\frac{1}{\sqrt{6}}$
$a, \Sigma^0 \rightarrow MB$	$-\frac{1}{\sqrt{2}}$	$\frac{1}{\sqrt{2}}$	0
$b, \Sigma^0 \rightarrow MB$	$\frac{1}{\sqrt{2}}$	$-\frac{1}{\sqrt{2}}$	$\frac{1}{\sqrt{2}}$

As in the last section, the isospin-zero channel is constructed from the particle channels according to

$$\begin{aligned}
|\pi \Sigma, I=0\rangle &= -\frac{1}{\sqrt{3}} |\pi^+ \Sigma^- \rangle - \frac{1}{\sqrt{3}} |\pi^0 \Sigma^0 \rangle - \frac{1}{\sqrt{3}} |\pi^- \Sigma^+ \rangle, \\
|\bar{K} N, I=0\rangle &= \frac{1}{\sqrt{2}} |\bar{K}^0 n \rangle + \frac{1}{\sqrt{2}} |K^- p \rangle.
\end{aligned} \quad (26)$$

By using the Feynman rules from Eq. (25) and from Eq. (19) for the γMM vertex, the amplitudes read

$$\begin{aligned}
(-it \cdot \boldsymbol{\epsilon})^{(I=0)}[\gamma \Lambda \rightarrow (\pi \Sigma) \xrightarrow{\Lambda^*} \pi \Sigma^*] &= 0, \\
(-it \cdot \boldsymbol{\epsilon})^{(I=0)}[\gamma \Lambda \rightarrow (\bar{K} N) \xrightarrow{\Lambda^*} \pi \Sigma^*] \\
&= \frac{e}{\sqrt{2}f_\pi} \left(\frac{D}{3} + F \right) \tilde{G}'_3 T^{(31)} \mathbf{S}^\dagger \cdot \boldsymbol{\epsilon}, \\
(-it \cdot \boldsymbol{\epsilon})^{(I=0)}[\gamma \Sigma^0 \rightarrow (\pi \Sigma) \xrightarrow{\Lambda^*} \pi \Sigma^*] \\
&= -\frac{4eF}{3f_\pi} \tilde{G}'_4 T^{(41)} \mathbf{S}^\dagger \cdot \boldsymbol{\epsilon}, \\
(-it \cdot \boldsymbol{\epsilon})^{(I=0)}[\gamma \Sigma^0 \rightarrow (\bar{K} N) \xrightarrow{\Lambda^*} \pi \Sigma^*] \\
&= \frac{e}{\sqrt{6}f_\pi} (F - D) \tilde{G}'_3 T^{(31)} \mathbf{S}^\dagger \cdot \boldsymbol{\epsilon},
\end{aligned} \quad (27)$$

with the channel ordering $i = 1, \dots, 4$ being $\pi \Sigma^*$, $K \Xi^*$, $\bar{K} N$, $\pi \Sigma$ as in the previous sections. As before, we have chosen $\pi \Sigma^*$ as the final state, which will become clear in Sec. IV when the coupled-channel scheme is matched with a formalism with explicit excitation of the resonance.

The loop function \tilde{G}'_i in Eq. (27) for the first loop is given by

$$\begin{aligned}
\tilde{G}'_i &= i \int \frac{d^4 q}{(2\pi)^4} \frac{\mathbf{q}^2}{(q-k)^2 - m_i^2 + i\epsilon} \frac{1}{q^2 - m_i^2 + i\epsilon} \\
&\times \frac{1}{P^0 - q^0 - E_i(\mathbf{q}) + i\epsilon} \frac{M}{E_i(\mathbf{q})} \left(\frac{\mathbf{q}^2}{q_{\text{on}}^2} \right), \quad (28)
\end{aligned}$$

which is similar to \tilde{G} from Eq. (23) up to a factor M/E from the nonrelativistic reduction of the baryon propagator and a factor $\mathbf{q}^2/q_{\text{on}}^2$. As in the case of the MB^* s -wave loops, the divergence in Eq. (28) is regularized by a cutoff whose value is obtained by matching the dimensional regularization and cutoff scheme of the meson-baryon d -wave loop at $s^{1/2} = 1520$ MeV, as explained following Eq. (22). With the subtraction constant from Refs. [10, 11], values for the cutoff of $\Lambda_{\bar{K}N} = 507$ MeV and $\Lambda_{\pi\Sigma} = 558$ MeV follow. In the following section we present the technical details that have led to Eqs. (27) and (28), projecting the meson-pole term over d waves and performing the angular integrations.

B. The spin-polarization structure of d -wave loops

The structure of the two p -wave couplings of the first loop in the fourth diagram of Fig. 2 is given by

$$\epsilon^\mu (2q - k)_\mu \boldsymbol{\sigma} \cdot (\mathbf{k} - \mathbf{q}), \quad (29)$$

where the meson momentum of the MBB vertex is given by $q - k$ and the two mesons in the γMM vertex are at momentum $q - k$ and q . As $\epsilon^0 = 0$ in Coulomb gauge, the spin structure takes the form $\boldsymbol{\epsilon} \cdot \mathbf{q}\boldsymbol{\sigma} \cdot \mathbf{q}$ (neglecting the photon momentum \mathbf{k} , which is small in the radiative decay). The d -wave structure obtained from $\sigma_i q_i \epsilon_j q_j \rightarrow \sigma_i \epsilon_j (q_i q_j - \frac{1}{3} \mathbf{q}^2 \delta_{ij})$ will combine with the d -wave structure $Y_2(\hat{\mathbf{q}})$ coming from the $\bar{K}N \rightarrow \pi \Sigma^*$ vertex to produce a scalar quantity after the loop integration is performed. (For the second loop, we choose the $\pi \Sigma^*$ channel in the following, but the calculations hold for any of the four channels in the second loop.)

We write

$$\sigma_i \epsilon_j (q_i q_j - \frac{1}{3} \mathbf{q}^2 \delta_{ij}) = A [\sigma \otimes \epsilon]_\mu^2 Y_2(\hat{\mathbf{q}}) |0\rangle, \quad (30)$$

which indicates that the two vector operators $\vec{\sigma}$ and $\vec{\epsilon}$ couple to produce an operator of rank 2, which couples to the spherical harmonic $Y_2(\hat{\mathbf{q}})$ to produce a scalar. The right-hand side can be written as

$$\begin{aligned} & A \sum_{\mu} (-1)^{\mu} [\sigma \otimes \epsilon]_{\mu}^2 Y_{2,-\mu}(\hat{\mathbf{q}}) \\ &= A \sum_{\mu, \alpha} (-1)^{\mu} Y_{2,-\mu}(\hat{\mathbf{q}}) \mathcal{C}(112; \alpha, \mu - \alpha) \sigma_{\alpha} \epsilon_{\mu - \alpha}, \end{aligned} \quad (31)$$

where \mathcal{C} denotes the Clebsch-Gordan coefficient. To find the value of A we take the matrix element of both sides of Eq. (30) between the states m and m' so that

$$\begin{aligned} \langle m | \sigma_i \epsilon_j (q_i q_j - \frac{1}{3} \mathbf{q}^2 \delta_{ij}) | m' \rangle &= A \sum_{\mu} (-1)^{\mu} Y_{2,-\mu}(\hat{\mathbf{q}}) \epsilon_{\mu - m + m'} \\ &\quad \times \mathcal{C}(112; m - m', \mu - m + m') \\ &\quad \times \mathcal{C}(\frac{1}{2} 1 \frac{1}{2}; m', m - m'), \end{aligned} \quad (32)$$

where we have used $\langle m | \sigma_{\alpha} | m' \rangle = \sqrt{3} \mathcal{C}(\frac{1}{2} 1 \frac{1}{2}; m', \alpha, m)$. Taking specific values of spin 1/2 components, m and m' , we obtain

$$A = \sqrt{\frac{8\pi}{15}} \mathbf{q}^2. \quad (33)$$

Following Ref. [10], we now include the $\bar{K}N \rightarrow \pi \Sigma^*$ vertex given by

$$\begin{aligned} -it_{\bar{K}N \rightarrow \pi \Sigma^*} &= -i\beta_{\bar{K}N} |\mathbf{q}|^2 \mathcal{C}(\frac{1}{2} 2 \frac{3}{2}; m, M - m) \\ &\quad \times Y_{2,m-M}(\hat{\mathbf{q}}) (-1)^{M-m} \sqrt{4\pi} \end{aligned} \quad (34)$$

so that the total spin structure of the d -wave loop in Fig. 2 is essentially given by

$$\begin{aligned} J &= \sum_m \int \frac{d\Omega_q}{4\pi} \langle m | \sigma_i \epsilon_j (q_i q_j - \frac{1}{3} \mathbf{q}^2 \delta_{ij}) | m' \rangle \\ &\quad \times \mathcal{C}(\frac{1}{2} 2 \frac{3}{2}; m, M - m) Y_{2,m-M}(\hat{\mathbf{q}}) (-1)^{M-m} \sqrt{4\pi}, \end{aligned} \quad (35)$$

where we have performed an average over the angles in the integration over the loop momentum q . Using Eqs. (32) and (33) we can write this as

$$\begin{aligned} J &= \sqrt{\frac{2}{3}} \mathbf{q}^2 (-1)^{1-M+m'} \epsilon_{m'-M} \sum_m \mathcal{C}(\frac{1}{2} 1 \frac{1}{2}; m', m - m') \\ &\quad \times \mathcal{C}(\frac{1}{2} 2 \frac{3}{2}; m, M - m) \mathcal{C}(121; m - m', M - m), \end{aligned} \quad (36)$$

where we have used the well-known relations

$$\int d\Omega_q Y_{2,-\mu}(\hat{\mathbf{q}}) Y_{2,m-M}(\hat{\mathbf{q}}) = (-1)^{\mu} \delta_{\mu, m-M}$$

and

$$\begin{aligned} \mathcal{C}(112; m - m', m' - M) &= (-1)^{1-m+m'} \sqrt{\frac{5}{3}} \\ &\quad \times \mathcal{C}(121; m - m', M - m). \end{aligned}$$

The product of three Clebsch-Gordan coefficients is then combined into a single one with a Racah coefficient, resulting in the identity

$$\begin{aligned} & \sum_m \mathcal{C}(\frac{1}{2} 1 \frac{1}{2}; m', m - m') \mathcal{C}(\frac{1}{2} 2 \frac{3}{2}; m, M - m) \\ & \quad \times \mathcal{C}(121; m - m', M - m) \\ &= -\sqrt{\frac{1}{2}} \mathcal{C}(\frac{1}{2} 1 \frac{3}{2}; m', M - m'), \end{aligned} \quad (37)$$

so that we finally have

$$J = \frac{1}{\sqrt{3}} \mathbf{q}^2 \mathbf{S}^{\dagger} \cdot \boldsymbol{\epsilon}. \quad (38)$$

This relation implies that for practical purposes we can use for the d -wave projection of the two p -wave vertices the simple form $\frac{1}{\sqrt{3}} \mathbf{q}^2 \mathbf{S}^{\dagger} \cdot \boldsymbol{\epsilon}$ and for the d -wave vertex of the $MB \rightarrow MB^*$ amplitude the factor $\beta_{\bar{K}N} \mathbf{q}^2$ and continue with the formalism exactly as in the s wave.

In the on-shell reduction scheme for the d -wave transitions in the generation of the Λ^* , the factor q_{on}^2 from the vertex is absorbed in the kernel V , as can be seen in Eq. (15). As we cannot perform this factorization for the first loop, we continue using the factor $\beta_{\bar{K}N} \mathbf{q}^2$ for the d -wave vertex in this loop but then have to divide by q_{on}^2 , which will cancel the q_{on}^2 in V or in the T matrix. Considering all these factors, we obtain Eq. (27) with \tilde{G}'_i given in Eq. (28).

IV. NUMERICAL RESULTS

In the previous sections the amplitudes for the processes $\gamma \Lambda \xrightarrow{\Lambda^*} \pi \Sigma^*$ and $\gamma \Sigma^0 \xrightarrow{\Lambda^*} \pi \Sigma^*$ have been determined and are written in terms of the $T^{(i)}$, the unitary solution of the BSE (11) for meson-baryon scattering with the transitions from channel i to the $\pi \Sigma^*$ final state. To determine the partial photon decay widths of the $\Lambda^*(1520)$, the $T^{(i)}$ is expanded around the pole in the complex scattering plane and can be written as

$$T^{(i)} = \frac{g_i g_{\pi \Sigma^*}}{\sqrt{s} - M_{\Lambda^*(1520)}}. \quad (39)$$

The matrix elements from Eqs. (24) and (27) with this replacement for $T^{(i)}$ are now identified with the resonant process in Fig. 3, which is written as

$$(-it \cdot \boldsymbol{\epsilon}) = (-i g_{\Lambda^* \pi \Sigma^*}) \frac{i}{\sqrt{s} - M_{\Lambda^*}} g_{\Lambda^* \gamma \Lambda(\Sigma^0)} \mathbf{S}^{\dagger} \cdot \boldsymbol{\epsilon}. \quad (40)$$

This identification allows us to write the effective $\Lambda^* \gamma \Lambda$ and $\Lambda^* \gamma \Sigma^0$ couplings, $g_{\Lambda^* \gamma \Lambda}$ and $g_{\Lambda^* \gamma \Sigma^0}$, in terms of the couplings

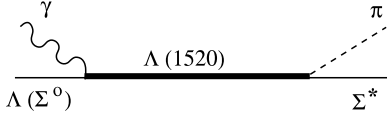


FIG. 3. Effective resonance representation of the radiative decay.

g_{i1} of the $\Lambda^*(1520)$ in the transition of the channel $i \rightarrow \Lambda^*(1520) \rightarrow \pi \Sigma^*$ with its values given in Table I, resulting in

$$\begin{aligned}
 g_{\Lambda^* \gamma \Lambda}^{(K \Xi^*)} &= -\frac{e}{2} \frac{f_{\pi N \Delta}^*}{m_\pi} \left(G_2 + \frac{2}{3} \tilde{G}_2 \right) g_{\Lambda^* K \Xi^*}, \\
 g_{\Lambda^* \gamma \Sigma^0}^{(\pi \Sigma^*)} &= -\frac{\sqrt{2}e}{3} \frac{f_{\pi N \Delta}^*}{m_\pi} \left(G_1 + \frac{2}{3} \tilde{G}_1 \right) g_{\Lambda^* \pi \Sigma^*}, \\
 g_{\Lambda^* \gamma \Sigma^0}^{(K \Xi^*)} &= \frac{e}{2\sqrt{3}} \frac{f_{\pi N \Delta}^*}{m_\pi} \left(G_2 + \frac{2}{3} \tilde{G}_2 \right) g_{\Lambda^* K \Xi^*}, \\
 g_{\Lambda^* \gamma \Lambda}^{(\bar{K} N)} &= \frac{e(D+3F)}{3\sqrt{2}f_\pi} \tilde{G}'_3 g_{\Lambda^* \bar{K} N}, \\
 g_{\Lambda^* \gamma \Sigma^0}^{(\pi \Sigma)} &= -\frac{4eF}{3f_\pi} \tilde{G}'_4 g_{\Lambda^* \pi \Sigma}, \\
 g_{\Lambda^* \gamma \Sigma^0}^{(\bar{K} N)} &= \frac{e(F-D)}{\sqrt{6}f_\pi} \tilde{G}'_3 g_{\Lambda^* \bar{K} N}.
 \end{aligned} \tag{41}$$

The upper index in parentheses indicates which particles are present in the first loop. Adding all processes, and using

$$\begin{aligned}
 g_{\Lambda^* \gamma \Lambda} &= g_{\Lambda^* \gamma \Lambda}^{(K \Xi^*)} + g_{\Lambda^* \gamma \Lambda}^{(\bar{K} N)}, \\
 g_{\Lambda^* \gamma \Sigma^0} &= g_{\Lambda^* \gamma \Sigma^0}^{(\pi \Sigma^*)} + g_{\Lambda^* \gamma \Sigma^0}^{(K \Xi^*)} + g_{\Lambda^* \gamma \Sigma^0}^{(\pi \Sigma)} + g_{\Lambda^* \gamma \Sigma^0}^{(\bar{K} N)},
 \end{aligned} \tag{42}$$

we find the partial decay width for the processes $\Lambda^*(1520) \rightarrow \gamma \Lambda$ and $\Lambda^*(1520) \rightarrow \gamma \Sigma^0$ to be given by

$$\Gamma = \frac{k}{3\pi} \frac{M_Y}{M_{\Lambda^*}} |g_{\Lambda^* \gamma Y}|^2, \tag{43}$$

where $Y = \Lambda, \Sigma^0$ is the final-state hyperon, and $k = \lambda^{1/2}(M_{\Lambda^*}, 0, M_Y^2)/(2M_{\Lambda^*})$ is the c.m. momentum of the decay products.

In Table IV the numerical results from this study are compared with experimental data.

For the $\gamma \Sigma^0$ final state, our result almost matches within errors the value given in Ref. [45], and it certainly matches it considering the theoretical uncertainties that we will estimate in the following. The experimental value from Ref. [45] is the only direct measurement of $\Gamma(\Lambda^* \rightarrow \gamma \Sigma^0)$. In the same experiment [45], the $\Gamma(\Lambda^* \rightarrow \gamma \Lambda)$ partial width has also been determined but it lies far below more recent measurements (see Table IV). Note that the value from Ref. [21] for $\Gamma(\Lambda^* \rightarrow \gamma \Sigma^0)$ is around six times larger than the value from Ref. [45]. However, this large value is not a direct measurement (see Ref. [48]) but is extrapolated from $\Gamma(\Lambda^* \rightarrow \gamma \Lambda)$ by using SU(3) arguments in Ref. [46]. In summary, the experimental situation is far from being clear. In the present study we compare to the direct measurement of $\Gamma(\Lambda^* \rightarrow \gamma \Sigma^0) = 47 \pm 17$ keV as a reference, but an independent experimental confirmation of this value would be desirable. Efforts in this direction have been announced [49]. It is also worth estimating the theoretical uncertainties. The largest source of uncertainty for us is the implicit use of SU(3) to relate the meson-baryon

TABLE IV. Experimental data, quark model results from Ref. [13,19], and results from this study for the partial decay width of the $\Lambda^*(1520)$ into $\gamma \Lambda$ and $\gamma \Sigma^0$. The results in brackets come from the use of empirical $\pi Y Y^*$ couplings or SU(3) uncertainties.

	$\Gamma[\Lambda^*(1520) \rightarrow \gamma \Lambda]$ (keV)	$\Gamma[\Lambda^*(1520) \rightarrow \gamma \Sigma^0]$ (keV)
From Ref. [45]	33 ± 11	47 ± 17
From Ref. [46]	134 ± 23	
From Ref. [47]	$159 \pm 33 \pm 26$	
From Ref. [12]	$167 \pm 43^{+26}_{-12}$	
From Ref. [13]	46	17
From Ref. [19]	258	157
This study	3 (2.5–4)	71 (60, with empirical $\Sigma^* \rightarrow \pi \Lambda, \pi \Sigma$ couplings)

octet-baryon decuplet couplings. We have scaled them to the $\pi N \Delta$ coupling. If we use the empirical couplings for $\Sigma^* \rightarrow \pi \Lambda, \pi \Sigma$ in agreement with the Σ^* partial decay widths, the value in parentheses in Table IV results.

The theoretical value for the $\gamma \Lambda$ final state in Table IV is systematically below experimental values although there are large discrepancies in the data. This suggests that the decay mechanisms could come from a different source than the coupled hadronic channels. The theoretical value is small because of large cancellations: In the scheme of dynamical generation, the dominant building channel of the $\Lambda^*(1520)$ is given by $\pi \Sigma^*$, as can be seen in Table I. However, in the isospin combination from Eq. (20), which is needed in Eq. (24), this channel precisely vanishes because of the cancellation of the $\pi^+ \Sigma^{*-}$ and $\pi^- \Sigma^{*+}$ contributions. The same holds for the $\pi \Sigma$ channel in the d wave with the cancellation in Eq. (27) from the isospin combination in Eq. (26). This channel is important because the branching ratio into $\pi \Sigma$ is large. In contrast, the diagrams with $\pi^+ \Sigma^{*-}$ and $\pi^- \Sigma^{*+}$ add in the $I = 0$ combination with $\gamma \Sigma^0$ in the final state instead of $\gamma \Lambda$, as Eq. (24) shows, and the same is true for $\pi \Sigma$ in the d wave. As a result, a much larger partial decay width for the $\gamma \Sigma^0$ final state is obtained.

The cancellation of the $\pi \Sigma$ and $\pi \Sigma^*$ channels can be also understood when we turn the external baryon line around and redraw the decay process as shown in Fig. 4.

First, we consider the case with the Λ . The $\pi^+ \pi^-$ system is necessarily in $J^P = 1^-$ as these are the quantum numbers of the photon. As a consequence, the condition $L + S + I =$

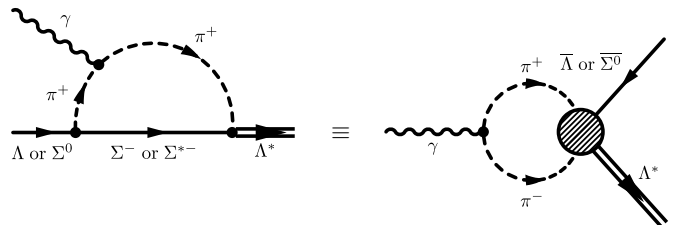


FIG. 4. Alternative representation of the photonic loop with $\pi \Sigma$ and $\pi \Sigma^*$.

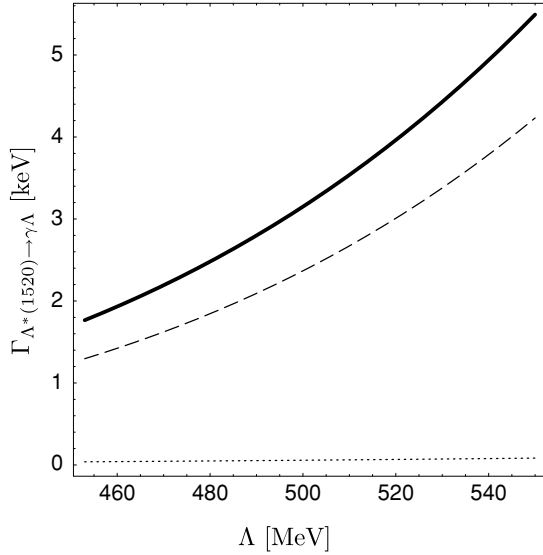


FIG. 5. Cutoff dependency of $\Gamma[\Lambda^*(1520) \rightarrow \gamma\Lambda]$ (in keV), showing contributions for different particles in the first loop and coherent sum. Dotted line: $K\Xi^*$ in the s wave. Dashed line: $\bar{K}N$ in the d wave. Thick solid line: coherent sum.

even for the two-pion state where $L = J = 1$ and $S = 0$ can only be fulfilled if the two-pion state is in $I = 1$; this is in contradiction to $I = 0$ of the $\bar{\Lambda}\Lambda^*$ system and is independent of the interaction, denoted with the gray dashed circle in Fig. 4. In contrast, if the baryon on the right side is a $\bar{\Sigma}^0$, then the $\bar{\Sigma}^0\Lambda^*$ system is in an isospin-one state, so a finite contribution is expected. If the $\pi^+\pi^-$ system is replaced with K^+K^- , there is no restriction imposed by $L + S + I = \text{even}$, so this process is possible for both Λ or $\bar{\Sigma}^0$ on the right side.

The situation is illustrated in Figs. 5 and 6, where the partial decay widths are plotted as a function of the cutoff in the first loops.

Indeed, the large $\pi\Sigma$ and $\pi\Sigma^*$ channels that contribute in Fig. 6 are missing in Fig. 5 and render the width small. Note also that the d -wave loops introduce a relatively strong cutoff dependence. Our cutoffs from Secs. III and III A have been uniquely fixed by matching the cutoff scheme to the dimensional regularization scheme of the MB^* and MB loop functions that generate dynamically the $\Lambda^*(1520)$. The latter have values for the subtraction constants that lead to a good data description in $\bar{K}N \rightarrow \bar{K}N$ and $\bar{K}N \rightarrow \pi\Sigma$ [11]. Therefore, if one assumes that the strong interaction in these processes fixes the cutoffs, their values should be taken seriously and not changed for the first loop with the photon. However, the strong cutoff dependence is a large source of theoretical error in the model of the radiative decay such that uncertainties as high as 50% would not be exaggerated. With this uncertainty the $\Lambda^*(1520) \rightarrow \gamma\Sigma^0$ is clearly compatible with the only data available. But the $\Lambda^*(1520) \rightarrow \gamma\Lambda$ is certainly not. However, the fact that the only measurement for $\Lambda^*(1520) \rightarrow \gamma\Sigma^0$ is done in an experiment where the $\Lambda^*(1520) \rightarrow \gamma\Lambda$ disagrees so strongly with other measurements calls for caution and further data on this decay rate are most needed.

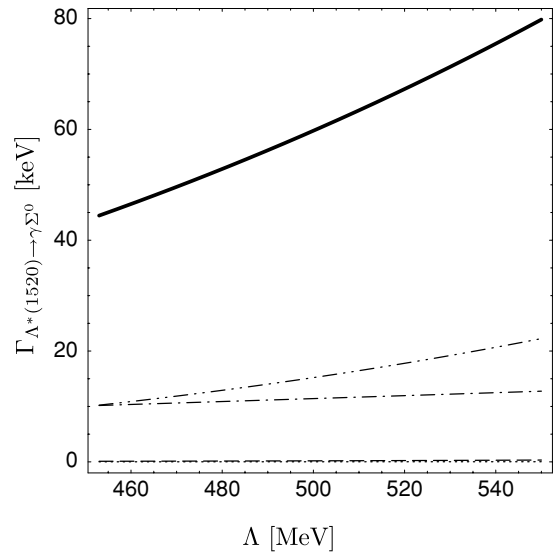


FIG. 6. Cutoff dependency of $\Gamma[\Lambda^*(1520) \rightarrow \gamma\Sigma^0]$ (in keV), showing contributions for different particles in the first loop and coherent sum. Dotted line: $K\Xi^*$ in the s wave. Dashed line: $\bar{K}N$ in the d wave. Dashed dotted line: $\pi\Sigma^*$ in the s wave. Double-dashed dotted line: $\pi\Sigma$ in the d wave. Thick solid line: coherent sum.

Nonetheless, even with large uncertainties our prediction for $\Lambda^*(1520) \rightarrow \gamma\Lambda$ is definitely small. Uncertainties from the implicit SU(3) use in the couplings are estimated of the order of 15%, resulting in the band for the partial decay rate shown in parentheses in Table IV. Hence we have pinned down an observable that is extremely sensitive to extra components of the $\Lambda^*(1520)$ resonance beyond the meson-baryon ones provided by the chiral unitary approach. The sensitivity shows up because of the exact cancellation of the contribution from the most important components provided by the chiral unitary approach.

V. ESTIMATES OF STRENGTH OF THE GENUINE RESONANCE COMPONENT

The usual way to include a genuine resonance in the chiral unitary approach is by introducing a CDD pole in the kernel of the interaction in the BSE. The residues of the pole stand for the strength of the coupling of this genuine resonance component to the meson-baryon states of our space. These couplings are unknown generally and fits to data are performed to determine them, which in some cases [26] turn out to be compatible with zero, thus giving an indication that the genuine component plays a minor role in the structure of the physical resonance, which then qualifies as a dynamically generated resonance. In the present case we have no such experimental information to determine the strength of the genuine component. The success of the meson-baryon components alone in the d -wave $\bar{K}N$ scattering indicates a small component of a genuine resonance, which, however, is essential to reproduce the $\Lambda^*(1520) \rightarrow \Lambda\gamma$ decay. Even if we could determine this small component of the CDD pole from scattering (which, because of its minor role played there, would have large uncertainties), this would not help us in determining the role played in the radiative

decay $\Lambda^*(1520) \rightarrow \Lambda\gamma$ since there is a new, independent, and unknown coupling of the CDD component to the photon. One has to find other methods here to make estimates of the strength of the genuine resonance in the physical $\Lambda^*(1520)$. Because of this problem, we shall make use of the results of quark models to try to make some rough estimate.

The first thing one must admit is that, with the large differences found for the decay rates in different quark models (see Table IV), the uncertainties in the estimates must be large. But even then, the exercise is worth doing and also brings light on how extra experimental data could help in this analysis. In the first step let us take as more significant the most recent results obtained in a relativistic quark model that has been proven to have large predictive power [18,19]. The decay rate obtained with this model is twice as big as that found by experiment. Second, for the extra component we are searching for, there is no need to take a quark wave function that is fitted to data to obtain optimal agreement with experiment, assuming that this is the only component of the wave function. Hence, we would rather search for a quark component with just as s quark in the $1p$ level and the u and d quarks in the $1s$ ground state coupled to isospin 0 (i.e., no configuration mixing).

This wave function would help us obtain larger results for the $\Lambda^*(1520) \rightarrow \Lambda\gamma$ whereas there would be no changes for the $\Lambda^*(1520) \rightarrow \Sigma\gamma$ transition, as we have pointed out before in the absence of configuration mixing. It is reasonable to assume that if all the strength of the configuration mixing wave function of [19] is put into this single component, the strength for $\Lambda^*(1520) \rightarrow \Lambda\gamma$ decay would increase and the new strength would be roughly of the order of the sum of strengths for $\Lambda^*(1520) \rightarrow \Lambda\gamma$ and $\Lambda^*(1520) \rightarrow \Sigma\gamma$ transitions obtained with the configuration mixing wave function. Next, we assume that the new contribution interferes constructively with the one from the meson-baryon component (although the interference is very small) and then we find that with 20% of the genuine quark wave function we can reproduce the experimental data for $\Lambda^*(1520) \rightarrow \Lambda\gamma$ without spoiling the agreement for $\Lambda^*(1520) \rightarrow \Sigma\gamma$, which would simply be reduced by 20%. This latter decay would be exclusively due to the meson-baryon component.

The former exercise should be improved in a more realistic approach. Indeed, it is well known from studies of the cloudy bag model [50] that in models where the meson cloud plays a role in the building up of the baryon, the size is mostly due to the meson cloud while the quarks are confined in a very small region. We would invoke this finding to suggest that, in a hybrid analysis for the $\Lambda^*(1520)$ resonance, the quarks would be confined in a small region, smaller than that assumed in quark models such as that in Ref. [19], where all the baryon properties are attributed to the quarks. By recalling that the coupling $\Lambda^*(1520) \rightarrow \Lambda\gamma$ (or analogous radiative baryon-baryon transitions) is proportional to the inverse of the radius or the quark core [51], a quark wave function with half the radius of that used in Ref. [19] would lead to twice the radiative coupling, and hence 5% of the quark wave function would suffice to explain the data.

Rough as the analysis is, it has the virtue of touching the sensitive points of a more thorough analysis that could be performed in the future when more data are available. These

new data would certainly be necessary, because with just one piece of information, the rate of $\Lambda^*(1520) \rightarrow \Lambda\gamma$, one has ambiguities in the size and strength, as we have seen in this exercise. Yet, the rough results indicate that one could indeed live with a small component of a genuine resonance and a large size of the meson-baryon component, which would justify the success of the meson cloud component alone in explaining the scattering data.

One could also suggest extra experiments that would help provide more information in the future. In the same spirit of the cloudy bag model, we recall that baryon form factors usually have two regions: one at small momentum transfers, which is dictated by the meson cloud, and another at larger momentum transfers, which is determined by the size and strength of the quark core. In this sense, future information from $\Lambda^*(1520) \rightarrow \Lambda e^+e^-$ would certainly bring new light into the issue. Increased photon fluxes or kaon fluxes in planned future facilities make this goal attainable. But extra information concerning the $\Lambda^*(1520)$, which is now largely studied in several laboratories, could help in the quest of determining the structure of this interesting resonance.

VI. CONCLUSIONS

The chiral unitary model for the $\Lambda^*(1520)$ has been extended to describe the radiative decay of the Λ^* . Study of the two decay modes into $\gamma\Lambda$ and $\gamma\Sigma^0$ can help us gain insight into the nature of the Λ^* , as to whether it is a genuine three-quark state, a dynamically generated resonance, or a mixture of both.

For the $\gamma\Sigma^0$ final state we have seen that the model of dynamical generation matches the empirical value, although there are certain theoretical uncertainties from the d -wave loops in the model. However, the good reproduction of the empirical value fits in the picture because the dominant channels of our coupled-channel model add up for this decay, and in some quark models, the dominant three-quark component for this decay is small. In contrast, we find very little contribution from our model for the $\gamma\Lambda$ final state owing to a cancellation of the dominant channels, so that this decay should be dominated by the genuine three-quark component in a more realistic picture of the $\Lambda^*(1520)$ as a hybrid with some three-constituent-quark component and a substantial meson-baryon cloud.

We have made rough estimates using present information from relativistic quark models that point in the direction that a small admixture of a genuine three-constituent-quark wave function could explain the data.

More precise experimental information and theoretical tools are needed to make more quantitative conclusions about the $\Lambda^*(1520)$, but the findings of the present study point in the direction of the Λ^* being a composite object of a genuine three-quark state and a dynamical resonance, with the first component dominating the $\Lambda^*(1520) \rightarrow \gamma\Lambda$ decay and the second the $\Lambda^*(1520) \rightarrow \gamma\Sigma^0$ decay. Extra experimental work, measuring other couplings of the $\Lambda^*(1520)$, such as the one to \bar{K}^* , as recently shown in Ref. [51], or the $\Lambda^*(1520) \rightarrow \Lambda e^+e^-$ reaction, would also bring relevant information on the nature of the $\Lambda^*(1520)$.

ACKNOWLEDGMENTS

We would like to thank D. Strottman for a thorough reading of the paper and B. Metsch for useful discussions. This work is partly supported by DGICYT Contract No. BFM2003-00856,

Generalitat Valenciana, and the E.U. EURIDICE network Contract No. HPRN-CT-2002-00311. This research is part of the EU Integrated Infrastructure Initiative Hadron Physics Project under Contract No. RII3-CT-2004-506078.

-
- [1] R. H. Dalitz and S. F. Tuan, *Ann. Phys.* **10**, 307 (1960).
 [2] B. K. Jennings, *Phys. Lett.* **B176**, 229 (1986).
 [3] N. Kaiser, P. B. Siegel, and W. Weise, *Phys. Lett.* **B362**, 23 (1995).
 [4] N. Kaiser, T. Waas, and W. Weise, *Nucl. Phys.* **A612**, 297 (1997).
 [5] E. Oset and A. Ramos, *Nucl. Phys.* **A635**, 99 (1998).
 [6] J. C. Nacher, A. Parreno, E. Oset, A. Ramos, A. Hosaka, and M. Oka, *Nucl. Phys.* **A678**, 187 (2000).
 [7] J. A. Oller and U. G. Meissner, *Phys. Lett.* **B500**, 263 (2001).
 [8] E. E. Kolomeitsev and M. F. M. Lutz, *Phys. Lett.* **B585**, 243 (2004).
 [9] S. Sarkar, E. Oset, and M. J. Vicente Vacas, *Nucl. Phys.* **A750**, 294 (2005).
 [10] S. Sarkar, E. Oset, and M. J. Vicente Vacas, *Phys. Rev. C* **72**, 015206 (2005).
 [11] L. Roca, S. Sarkar, V. K. Magas, and E. Oset, *Phys. Rev. C* **73**, 045208 (2006).
 [12] S. Taylor *et al.* (CLAS Collaboration), *Phys. Rev. C* **71**, 054609 (2005); **72**, 039902(E) (2005).
 [13] E. Kaxiras, E. J. Moniz, and M. Soyeur, *Phys. Rev. D* **32**, 695 (1985).
 [14] J. W. Darewych, M. Horbatsch, and R. Koniuk, *Phys. Rev. D* **28**, 1125 (1983).
 [15] M. Warns, W. Pfeil, and H. Rollnik, *Phys. Lett.* **B258**, 431 (1991).
 [16] Y. Umino and F. Myhrer, *Nucl. Phys.* **A529**, 713 (1991).
 [17] Y. Umino and F. Myhrer, *Nucl. Phys.* **A554**, 593 (1993).
 [18] T. Van Cauteren, D. Merten, T. Corthals, S. Janssen, B. Metsch, H. R. Petry, and J. Ryckebusch, *Eur. Phys. J. A* **20**, 283 (2004).
 [19] T. Van Cauteren, J. Ryckebusch, B. Metsch, and H. R. Petry, *Eur. Phys. J. A* **26**, 339 (2005).
 [20] R. Bijker, F. Iachello, and A. Leviatan, *Ann. Phys. (NY)* **284**, 89 (2000).
 [21] S. Eidelman *et al.* (Particle Data Group), *Phys. Lett.* **B592**, 1 (2004).
 [22] E. Jenkins and A. V. Manohar, *Phys. Lett.* **B259**, 353 (1991).
 [23] G. F. Chew and F. E. Low, *Phys. Rev.* **101**, 1570 (1956).
 [24] U. G. Meissner and J. A. Oller, *Nucl. Phys.* **A673**, 311 (2000).
 [25] L. Castillejo, R. H. Dalitz, and F. J. Dyson, *Phys. Rev.* **101**, 453 (1956).
 [26] J. A. Oller and E. Oset, *Phys. Rev. D* **60**, 074023 (1999).
 [27] D. J. Ernst, *Phys. Rev. C* **64**, 035201 (2001).
 [28] R. F. Dashen, E. Jenkins, and A. V. Manohar, *Phys. Rev. D* **49**, 4713 (1994); **51**, 2489(E) (1995).
 [29] C. L. Schat, J. L. Goity, and N. N. Scoccola, *Phys. Rev. Lett.* **88**, 102002 (2002).
 [30] T. D. Cohen and R. F. Lebed, *Phys. Rev. Lett.* **91**, 012001 (2003).
 [31] T. D. Cohen and R. F. Lebed, *Phys. Rev. D* **68**, 056003 (2003).
 [32] J. R. Pelaez, *Phys. Rev. Lett.* **92**, 102001 (2004).
 [33] F. Gross and Y. Surya, *Phys. Rev. C* **47**, 703 (1993).
 [34] Y. Surya and F. Gross, *Phys. Rev. C* **53**, 2422 (1996).
 [35] D. Jido, E. Oset, and A. Ramos, *Phys. Rev. C* **66**, 055203 (2002).
 [36] A. D. Lahiff and I. R. Afnan, *Phys. Rev. C* **66**, 044001 (2002).
 [37] S. Kondratyuk, A. D. Lahiff, and H. W. Fearing, *Phys. Lett.* **B521**, 204 (2001).
 [38] M. F. M. Lutz and E. E. Kolomeitsev, *Nucl. Phys.* **A700**, 193 (2002).
 [39] M. N. Butler, M. J. Savage, and R. P. Springer, *Nucl. Phys.* **B399**, 69 (1993).
 [40] E. E. Kolomeitsev and M. F. M. Lutz, *Phys. Lett.* **B585**, 243 (2004).
 [41] B. Borasoy, P. C. Bruns, U. G. Meißner, and R. Nißler, *Phys. Rev. C* **72**, 065201 (2005).
 [42] M. Döring, E. Oset, and D. Strottman, *Phys. Rev. C* **73**, 045209 (2006).
 [43] J. Gasser and H. Leutwyler, *Nucl. Phys.* **B250**, 465 (1985).
 [44] E. Oset and A. Ramos, *Nucl. Phys.* **A679**, 616 (2001).
 [45] R. Bertini, *Nucl. Phys.* **B279**, 49 (1987); R. Bertini *et al.*, SACLAY-DPh-N-2372 (unpublished).
 [46] T. S. Mast, M. Alston-Garnjost, R. O. Bangerter, A. Barbaro-Galtieri, L. K. Gershwil, F. T. Solmitz, and R. D. Tripp, *Phys. Rev. Lett.* **21**, 1715 (1968).
 [47] Y. M. Antipov *et al.* (SPHINX Collaboration), *Phys. Lett.* **B604**, 22 (2004).
 [48] Y. Oh, K. Nakayama, and T. S. Lee, paper presented at Workshop on the Physics of Excited Nucleons (NSTAR 2005), Tallahassee, Florida, 12–15 October 2005, arXiv:hep-ph/0511198.
 [49] D. V. Vavilov *et al.* (SPHINX Collaboration), *Phys. At. Nucl.* **68**, 378 (2005).
 [50] A. W. Thomas, S. Theberge, and G. A. Miller, *Phys. Rev. D* **24**, 216 (1981).
 [51] T. Hyodo, S. Sarkar, A. Hosaka, and E. Oset, *Phys. Rev. C* **73**, 035209 (2006).